On Parameterization of Heat Conduction in Coupled Soil Water and Heat Flow Modelling

Jana VOTRUBOVÁ[1], Michal DOHNAL[1], Tomáš VOGEL[1] and Miroslav TESAŘ[2]

[1]Faculty of Civil Engineering, Czech Technical University in Prague, Prague, Czech Republic;
[2]Institute of Hydrodynamics of the ASCR, Prague, Czech Republic

Abstract: Soil water and heat transport plays an important role in various hydrologic, agricultural, and industrial applications. Accordingly, an increasing attention is paid to relevant simulation models. In the present study, soil thermal conditions at a mountain meadow during the vegetation season were simulated. A dual-continuum model of coupled water and heat transport was employed to account for preferential flow effects. Data collected at an experimental site in the Šumava Mountains, southern Bohemia, during the vegetation season 2009 were employed. Soil hydraulic properties (retention curve and hydraulic conductivity) determined by independent soil tests were used. Unavailable hydraulic parameters were adjusted to obtain satisfactory hydraulic model performance. Soil thermal properties were estimated based on values found in literature without further optimization. Three different approaches were used to approximate the soil thermal conductivity function, λ(θ): (*i*) relationships provided by Chung and Horton (*ii*) linear estimates as described by Loukili, Woodbury and Snelgrove, (*iii*) methodology proposed by Côté and Konrad. The simulated thermal conditions were compared to those observed. The impact of different soil thermal conductivity approximations on the heat transport simulation results was analysed. The differences between the simulation results in terms of the soil temperature were small. Regarding the surface soil heat flux, these differences became substantial. More realistic simulations were obtained using λ(θ) estimates based on the soil texture and composition. The differences between these two, related to neglecting vs. considering λ(θ) non-linearity, were found negligible.

Keywords: advective heat flux; dual-permeability model; preferential flow; soil heat transport; soil thermal conductivity; surface energy balance

Soil thermal conditions and heat fluxes affect a wide range of processes of interest in various fields of geosciences. Thus the soil heat transport simulation is becoming an integral part of models describing diverse phenomena: the land surface influence on climate and meteorological conditions (Loukili *et al*. 2008), crop growth (Timlin *et al*. 2002), soil CO_2 production (Buchner *et al*. 2008; Bauer *et al*. 2012), ecosystem carbon sequestration (Ju *et al*. 2006), or subsurface soil water evaporation (Sakai *et al*. 2011). The coupled soil water and heat transport modelling was also used to improve the understanding of hydraulic processes below the land surface (Ronan *et al*. 1998; Vogel *et al*. 2011).

Usually, the soil heat transport simulations are based on estimates of the soil thermal conductivity as a function of the soil water content, λ(θ). In many studies (Buchner *et al*. 2008; Bauer *et al*. 2012; Sakai *et al*. 2011) the λ(θ) relationships published by Chung and Horton (1987) are employed; even though they were introduced as λ(θ) approximations for the three soils studied, not as estimates to be used for different soils. The λ(θ) estimation methods assess the soil thermal conductivity in dry and saturated soil conditions using the basic knowledge of the soil composition, and then approximate the shape of the λ(θ) relationship. Some models rely on a simple linear λ(θ) relationship (Loukili *et al*. 2008). More

sophisticated methods provide non-linear λ(θ) estimates. Of these, Côté and Konrad (2005) methodology has recently been employed (Ju *et al*. 2006; Vogel *et al*. 2011).

In the present study, the effect of using various λ(θ) approximations on simulated soil thermal conditions is tested. The soil water content and temperature in a mountain meadow during the vegetation season 2009 are simulated. One-dimensional dual-continuum model of coupled water and heat transport is employed (Vogel *et al*. 2011). The soil thermal conductivity is assessed using three different approaches: (*i*) relationships provided by Chung and Horton (1987), (*ii*) linear λ(θ) estimates as described by Loukili *et al*. (2008), (*iii*) methodology proposed by Côté and Konrad (2005). The results of simulations are compared with the soil temperatures observed and performance of the different λ(θ) approximation methods is examined. The impact of preferential flow and root water uptake is also discussed.

MATERIAL AND METHODS

Experimental site and data collected

The Liz experimental site is located near a small headwater catchment of the same name in the Volyňka river basin, Šumava Mountains, southern Bohemia. The site has been used for long-term monitoring of micrometeorological and hydrological variables (Tesař *et al*. 2006). It is situated on a meadow of mild slope at an altitude of 830 m a.s.l. The mean annual temperature is 6.3°C, the mean annual precipitation is 861 mm. The soil is Cambisol developed upon the biotite paragneiss bedrock. It is coarse sandy loam (1-m deep) over the weathered bedrock. The groundwater table is about 8 m below the surface. The grass is mowed several times a year.

The micrometeorological conditions are monitored continuously with a 15-min time step. Variables used in the present study include rainfall intensity, air temperature, air humidity, barometric pressure, wind speed, and radiation. The thermal conditions below the soil surface are observed with the same temporal resolution using Pt100 soil temperature sensors inserted at 5 different depths below the soil surface (5, 10, 20, 50, and 100 cm). There is one sensor placed at each depth. The hydraulic conditions within the soil are monitored with pressure transducer tensiometers inserted at 5 different depths (15, 30, 45, 60, and 90 cm), each depth being equipped with 2–3 sensors. The soil water pressure data are collected manually 3 times a week.

The soil hydraulic properties were examined using standard tests. The soil water retention curves were measured for 100-ccm samples taken at 4 depths below the surface (15, 30, 45, and 60 cm) using the pressure plate method. The unsaturated hydraulic conductivity for the pressure head of –3 cm was determined using in-situ minidisk-infiltrometer measurements and the empirical relationship proposed by Dohnal *et al*. (2010). The presence and character of the preferential flow were demonstrated by means of a dye tracer applied during an in-situ ponded infiltration experiment (Císlerová 2005).

Simulation model

The dual-continuum modelling approach was used in the present study. This modelling concept has proved useful for simulating water and solute transport in soils with preferential flow behaviour. It is based on the assumption that the soil water flow takes place in a system of two parallel, mutually communicating flow domains: the soil matrix domain (further abbreviated to SM-domain) and the preferential flow domain (denoted as PF-domain).

The variably saturated vertical flow of water is described by a dual set of one-dimensional Richards' equations. These equations are coupled through a first-order soil water transfer term, which enables dynamic exchange of water between the PF-domain and the SM-domain. The governing equations, based on the concept of Gerke and van Genuchten (1993), are formulated in a similar way like in Vogel *et al.* (2010):

$$\frac{\partial w_f \theta_f}{\partial t} = \frac{\partial}{\partial z}\left(w_f K_f \left(\frac{\partial h_f}{\partial z} + 1 \right) \right) - w_f S_f - \alpha_{ws} K_{ar} (h_f - h_m) \quad (1)$$

$$\frac{\partial w_m \theta_m}{\partial t} = \frac{\partial}{\partial z}\left(w_m K_m \left(\frac{\partial h_m}{\partial z} + 1 \right) \right) - w_m S_m + \alpha_{ws} K_{ar} (h_f - h_m) \quad (2)$$

where:

m – denotes the SM-domain variables

f – denotes the PF-domain variables

i = f or m

w_i – volumetric fractions of the soil occupied by the respective flow domain (fulfilling the condition $w_m + w_f = 1$)
h_i – domain specific soil water pressure head (m)
K_i – unsaturated hydraulic conductivity (m/s)
θ_i – volumetric soil water content (–)
S_i – intensity of the root water uptake due to transpiration (1/s)
α_{ws} – interdomain soil water transfer coefficient at saturation (1/m/s)
K_{ar} – relative unsaturated hydraulic conductivity of the SM-domain/PF-domain interface

The transient exchange of water between the two flow domains is represented by the first-order soil water transfer term, Γ_w, expressed by the last term of Eqs (1) and (2).

The heat transport in this dual-continuum system is described by the following set of governing equations (Vogel *et al*. 2011):

$$\frac{\partial w_f C_f T_f}{\partial t} = -\frac{\partial w_f q_f C_w T_f}{\partial z} + \frac{\partial}{\partial z}\left(w_f \lambda^*_f \frac{\partial T_f}{\partial z}\right) - w_f S_f C_w T_f - \Gamma_H \quad (3)$$

$$\frac{\partial w_m C_m T_m}{\partial t} = -\frac{\partial w_m q_m C_w T_m}{\partial z} + \frac{\partial}{\partial z}\left(w_m \lambda^*_m \frac{\partial T_m}{\partial z}\right) - w_m S_m C_w T_m + \Gamma_H \quad (4)$$

where:
T_i – domain specific temperature (K)
C_i – volumetric heat capacity of soil (J/m^3/K)
C_w – volumetric heat capacity of water (J/m^3/K)
q_i – soil water flux (m/s)
λ^*_i – soil apparent thermal conductivity (W/m/K)
Γ_H – interdomain heat transfer term (W/m^3)

The heat flux directed from one domain to the other is evaluated using a simple first-order formula accounting for both advective and conductive heat exchange:

$$\Gamma_H = \Gamma_w C_w T_w + \frac{\tau}{\Delta}\lambda_a (T_f - T_m) \quad (5)$$

where:
T_w – temperature of water being exchanged between domains (K)
τ – specific interfacial area (1/m)
Δ – characteristic length associated with the interdomain heat transfer (m)
λ_a – effective thermal conductivity of the SM-domain/PF-domain interface

More details on the interdomain heat transfer parameterization can be found in Vogel *et al*. (2011).

The domain specific volumetric heat capacities, C_f and C_m, can be calculated from the soil composition (de Vries 1963):

$$C_i = \varepsilon_{si} C_{si} + \varepsilon_{oi} C_{oi} + \theta_i C_w \quad (6)$$

where:
C_{si}, C_{oi}, C_w – volumetric heat capacities of inorganic solid matter, organic matter and water (J/m^3/K)
ε_{si}, ε_{oi}, θ_i – respective volumetric fractions of the substances

The soil apparent thermal conductivities, λ^*_f and λ^*_m, are estimated according to

$$\lambda^*_i = \lambda_i(\theta_i) + C_w |q_i| d_i \quad (7)$$

where:
$\lambda_i(\theta_i)$ – soil thermal conductivity function (W/m/K), expressing the λ-θ relationship for variably saturated conditions
d_i – thermal dispersivity (m), which plays a similar role in the heat transport model as does the mechanical dispersivity in the solute transport model (de Marsily 1986)

The above governing equations for soil water flow and heat transport are solved numerically using the finite element method. The numerical solver is implemented in the dual-continuum model S1D developed at CTU Prague. More details about the S1D code can be found in Vogel *et al*. (2010).

Results of the heat transport model can be interpreted in terms of either soil temperature or soil heat storage and fluxes. The local soil heat flux in each flow domain, j_i (W/m^2), consists of two components representing heat advection and heat conduction:

$$j_i = q_i C_w T_i - \lambda^*_i \frac{\partial T_i}{\partial z} \quad (8)$$

The composite soil heat flux is calculated according to

$$j = w_f j_f + w_m j_m \quad (9)$$

Similarly, the composite volumetric soil heat storage, H (J/m^3), is related to the domain specific heat storages through

$$H = w_f C_f T_f + w_m C_m T_m \quad (10)$$

When evaluated for the soil-atmosphere boundary, the soil conductive heat flux, j, represents Q_G component of the surface energy balance formulated for the atmospheric side of the boundary:

$$R_n = Q_L + Q_H + Q_G \quad (11)$$

where:
R_n – net radiation (W/m^2)
Q_L – latent heat flux (W/m^2)
Q_H – sensible heat flux (W/m^2)
Q_G – soil heat flux (W/m^2)

Soil hydraulic parameters

The soil profile was divided into 6 layers (Table 1). The upper 10-cm layer describes the grass root zone. The next four layers, to the depth of 100 cm, are divided according to the retention-curve sampling depths. The bottom layer between 100 and 300 cm represents underlying material identified as coarse debris with silty-sand filling.

The soil hydraulic properties were described using the modified van Genuchten-Mualem approach which accounts for non-zero air-entry value, h_s (Vogel *et al.* 2001). The values of the employed parameters are given in Table 1. Results of the laboratory retention curve measurements and in-situ minidisc-infiltration experiments were used to describe the SM-domain hydraulic properties at depths between 10 and 100 cm (K_s was assumed equal to the hydraulic conductivity obtained for h = –3 cm). In the upper 10-cm layer of SM-domain, the parameters were set similar to those used for the grass root zone in Vogel *et al.* (2010) as no experimental data are available for this horizon. The PF-domain hydraulic properties were described by parameters characteristic of sandy soil in order to mimic the fast preferential flow effective only under close-to-saturation conditions. The PF-domain fraction (Table 2) was assessed based on simple visual examination of the results of in-situ dye tracer experiment. The hydraulic properties of SM-domain in the remaining lower part of the profile were manually adjusted to assure the retention of soil water within the upper 100-cm soil layer, as indicated by the pressure head measurements. The interdomain water transfer (represented by α_{ws} values) was manually adjusted so that a satisfactory pressure head simulation within the upper 100-cm soil layer was obtained.

Soil thermal parameters

The soil thermal properties affecting the heat transport were estimated based on information available in literature. The volumetric heat capacities of separate soil constituents were considered to be C_{water} = 4.2 × 10^6, $C_{mineral}$ = 2.3 × 10^6, and $C_{organic}$ = 2.5 × 10^6 J/m^3/K (e.g. Hillel 1998). The bulk soil heat capacity was calculated as the volume-weighted mean of these values according to the actual soil composition (Eq. (6)). The volumetric fractions of the soil solid constituents ($\varepsilon_{mineral}$, $\varepsilon_{organic}$) are shown in Table 1.

Table 1. Model flow domain properties

Domain	Depth (cm)	θ_r	θ_s	α (1/cm)	n (–)	K_s (cm/day)	h_s (cm)	$\varepsilon_{mineral}$	$\varepsilon_{organic}$
		(–)						(–)	
SM-domain	0–10	0.36	0.62	0.050	2.00	100.0	–1.8	0.28	0.10
	10–20	0.25	0.45	0.016	1.49	3.0	–3.5	0.51	0.04
	20–35	0.24	0.42	0.022	1.45	2.5	–3.2	0.56	0.02
	35–50	0.15	0.39	0.024	1.25	2.5	–2.1	0.60	0.01
	50–100	0.19	0.39	0.011	1.59	2.0	–2.1	0.61	0
	100–300	0.07	0.27	0.060	1.48	0.5	–1.1	0.73	0
PF-domain	0–10	0.05	0.43	0.144	2.68	2000	–0.8	0.47	0.10
	10–300	0.05	0.43	0.144	2.68	1000	–0.8	0.57	0

θ_r – residual water content; θ_s – saturated water content; h_s – air-entry value; α, n – retention curve shape parameters; K_s – saturated hydraulic conductivity; $\varepsilon_{mineral}$, $\varepsilon_{organic}$ – soil constituent fraction; note that $\varepsilon_{mineral} + \varepsilon_{organic} + \theta_s = 1$

Table 2. Model PF-domain distribution and interdomain communication

Depth (cm)	w_f (–)	α_{ws} (1/cm/day)	τ/Δ (1/cm^2)
0	0.30	0.10	0.01
10	0.20	0.10	0.01
100	0.05	0.05	0.01
300	0.05	0.05	0.01

w_f – PF-domain fraction; α_{ws} – interdomain soil water transfer coefficient at saturation; τ/Δ – the ratio of specific surface to effective distance

The bulk soil thermal conductivities as functions of the soil water contents, $\lambda(\theta)$, were estimated using three different approaches. Their concepts are described below and illustrated in Figure 1. An overview of the resulting thermal conductivity functions obtained for the soil profile studied is presented in Figure 2. Wherever applicable, the soil constituent thermal conductivities were assumed to be $\lambda_{water} = 0.57$, $\lambda_{mineral} = 2.60$, and $\lambda_{organic} = 0.25$ W/m/K (Côté & Konrad 2005)

Firstly, the expression published by Chung and Horton (1987) was considered (C&H):

$$\lambda(\theta) = b_1 + b_2\theta + b_3\theta^{0.5} \quad (12)$$

where:

b_1, b_2, b_3 – empirical parameters (W/m/K)

The values of b_1, b_2, b_3, determined based on experimental data for three soils were also provided: –0.197, –0.962, and 2.521 W/m/K for clay; 0.243, 0.393, and 1.534 W/m/K for loam; 0.228, –2.406, and 4.909 W/m/K for sand (Figure 1a). Although these $\lambda(\theta)$ represent specific soils for which the measurements had been conducted by Chung and Horton (1987), they are often used as $\lambda(\theta)$ estimates for other soils based on their texture. Adopting this simple approach in the present study, the thermal conductivity function for loam was used within the SM-domain, and that for sand was applied within the PF-domain.

Secondly, the linear relationship presented by Loukili *et al.* (2008) was tested (LWS):

$$\lambda(\theta) = \lambda_{dry} + (\lambda_{sat} - \lambda_{dry})\, S_r \quad (13)$$

where:

λ_{dry}, λ_{sat} – soil thermal conductivities for dry and saturated soil, respectively

S_r – soil water saturation degree (equal to θ/θ_s)

In this case (Figure 1b), the thermal conductivity of dry soil is set equal to 0.275 W/m/K and that of the saturated soil is calculated as the volume-weighted geometric mean of thermal conductivities of all soil constituents, j (i.e. water, mineral, and organic):

$$\lambda_{sat} = \prod_j \lambda_j^{\varepsilon_j} = \lambda_{water}^{\theta_s}\, \lambda_{mineral}^{\varepsilon_{mineral}}\, \lambda_{organic}^{\varepsilon_{organic}} \quad (14)$$

Thirdly, the method proposed by Côté and Konrad (2005) was implemented (C&K). This method produces a nonlinear $\lambda(\theta)$ based on the knowledge of the soil composition and texture (Figure 1c). The relationship between the soil water content and the soil thermal conductivity is approximated by

$$\lambda = \lambda_{dry} + \left(\lambda_{sat} - \lambda_{dry}\right)\frac{\kappa S_r}{1 + (\kappa - 1)S_r} \quad (15)$$

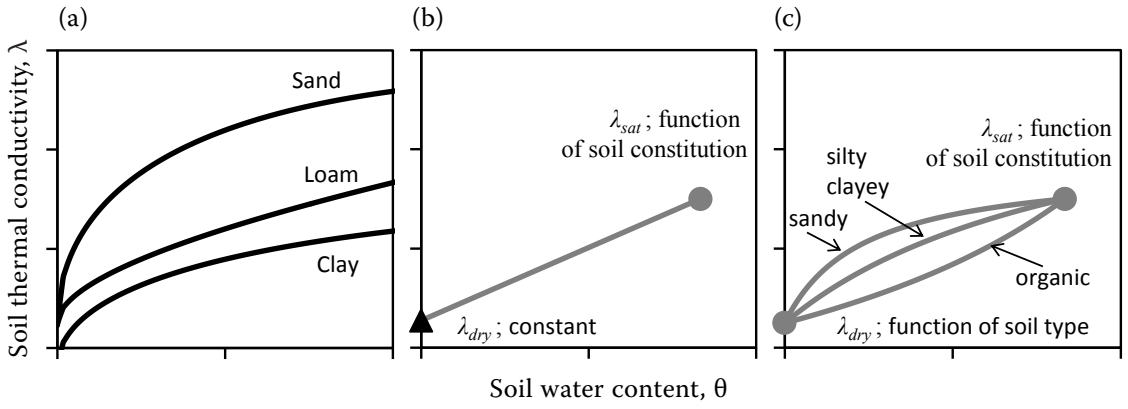

Figure 1. Schematic of three methods of the soil thermal conductivity estimation: (a) Chung and Horton (1987) (C&H), (b) Loukili *et al.* (2008) (LWS), (c) Côté and Konrad (2005) (C&K)

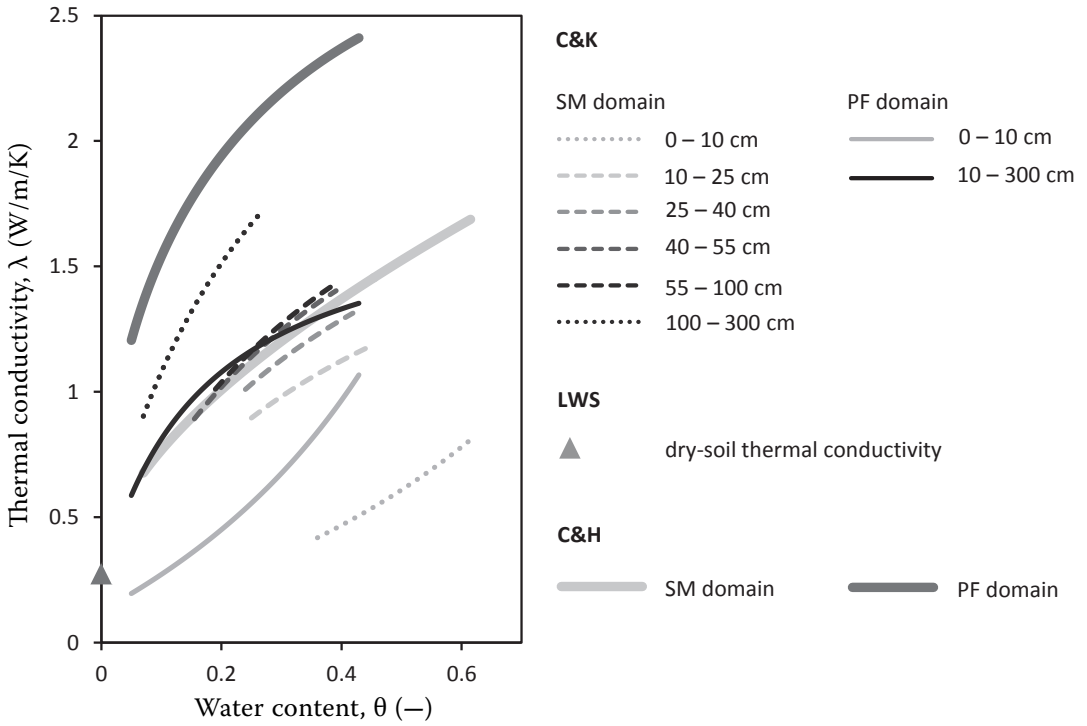

Figure 2. Relationships of bulk soil thermal conductivity to soil water content, λ(θ), as obtained by three different approximation methods; λ(θ) for each particular soil layer is plotted within the water content range between residual and saturated water contents, as given in Table 1; to each C&K λ(θ) approximation, there is a linear LWS λ(θ) estimate related that would show as a straight line (not presented) connecting the C&K λ(θ) maximum with the λ_{dry} (depicted by the triangle)

$$\lambda_{dry} = \chi \times 10^{\eta n} \quad (16)$$

where:

n – soil porosity

κ, χ (W/m/K), η – empirical parameters dependent on the soil texture and composition (i.e. mineral soil vs. organic soil)

Values of these parameters relevant to various soil types were provided by Côté and Konrad (2005). In the present study, parameters for organic soils (0.60, 0.30 W/m/K and 0.87, respectively) were used within the upper 10-cm layer of each flow domain, those for natural mineral soils (1.90, 0.75 W/m/K and 1.20, respectively) within the rest of the SM-domain, and those for sands (3.55, 0.75 W/m/K and 1.20, respectively) within the rest of the PF-domain. Regarding λ_{sat}, it is estimated in the same way as for the LWS method (Eq. (14)).

The soil thermal dispersivities, d_m and d_f, were set equal to 5 cm. The ratio of specific surface to effective distance, τ/Δ, which controls the inter-domain conductive heat exchange (via Γ_H), was adjusted within its estimated range to ensure stable simulation (Table 2).

Boundary and initial conditions

Soil water flow and heat transport during the vegetation season of 2009 (May 30–October 12) were simulated. The initial conditions were set according to the soil water pressure and the soil temperature observed.

The upper boundary conditions (Figure 3) were given by the rainfall intensities observed (prescribed flux boundary condition) and by the surface temperature calculated from the observed long-wave radiation emitted by the soil and vegetation surface, L_G (prescribed resident temperature condition). The Stefan-Boltzmann law ($L_G = \sigma \times T^4$) under the black-body approximation ($\sigma = 5.67 \times 10^{-8}$ W/m^2/K^4) was used.

At the bottom boundary, the free drainage condition (equivalent to the unit hydraulic gradient condition) was used for the water flow simula-

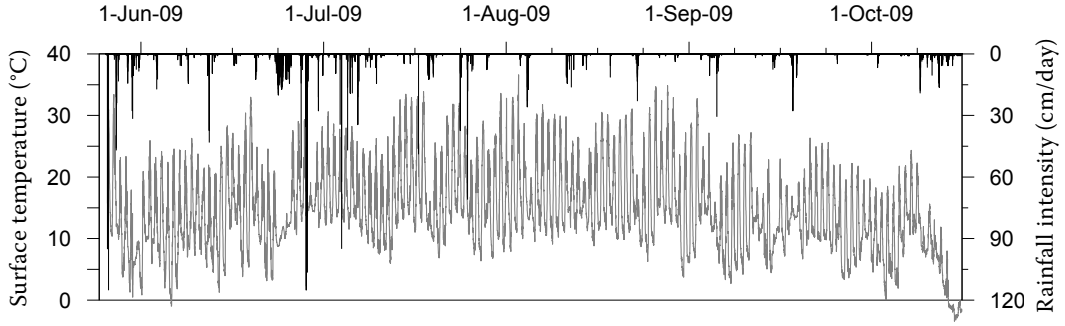

Figure 3. Upper boundary conditions of the simulation: surface temperature (grey) and rainfall intensity (black), both given with 15-minute time step

tion, while the zero thermal gradient (Neumann boundary condition) was assigned for the heat transfer simulation.

The hourly potential evapotranspiration rate was estimated using the Penman-Monteith (PM) formula (Monteith 1981):

$$E = \frac{1}{L\rho_w} Q_L = \frac{1}{L\rho_w} \frac{(R_n - Q_G)\delta + \rho_a c_p (p_{vs} - p_v)/r_a}{\delta + \gamma(1 + r_s/r_a)} \quad (17)$$

where:

E – evapotranspiration rate (m/s)
L – specific latent heat of vaporization (J/kg)
ρ_w, ρ_a – densities of water and air (kg/m^3)
δ – slope of the saturation vapour pressure curve (Pa/K)
c_p – specific isobaric heat capacity of air (J/kg/K)
$p_{vs}-p_v$ – vapour pressure deficit (Pa)
r_s, r_a – surface and aerodynamic resistances (s/m)
γ – psychrometric constant (Pa/K)

The formula was applied to hour-averaged data. Q_G was approximated as a fraction of the net radiation, specifically, 0.1 × R_n for daylight hours and 0.5 × R_n at night (Allen *et al.* 1998).

The actual root water uptake was modelled using the approach of Feddes *et al.* (1978). The plant water stress function was approximated by a standard trapezoidal shape. The optimum water uptake rate, implying stress-free conditions, was assumed for the local soil water pressure higher than –600 cm. Between this pressure and the wilting point, which was set equal to –12 000 cm, linear reduction of the water uptake was prescribed. The water uptake was applied to the SM-domain only. It was distributed over the upper 40 cm of the soil profile decreasing linearly with depth.

RESULTS AND DISCUSSION

The overview of the water flow simulation results is given in Figure 4. The soil water pressure head simulated in the SM-domain is compared with that observed. The simulation started at relatively saturated conditions (soil water pressure close to zero). After a drought period (pressure decrease), major rainfall events occurred at the end of June and at the beginning of July that immediately affected the whole soil profile monitored (pressure head reaching zero or even positive values). Periodic drying and wetting cycles followed. In August and early September, the soil water pressure head gradually decreased as the evapotranspiration was counterbalanced by precipitation only partially. The accumulated moisture loss was eventually compensated by the rainfall event in mid-September. Subsequently, one more cycle of soil drying and wetting was observed. At the end of the period studied, the soil water pressure conditions were close to those at the beginning.

The agreement of model results with the soil water pressure observed is considered as reasonably good. This was achieved mainly by optimizing the hydraulic properties of the bottom-most layer. It might be possible to further improve this agreement by optimizing the hydraulic parameters of the upper soil layers. In the present study, these parameters were set according to the soil test results.

In Figure 5, the primary results of the coupled water and heat transport simulation are shown. The temporal changes of the soil temperature distribution as obtained for the upper 100-cm soil profile using C&K method of thermal conductivity estimation are presented. Both daily and seasonal temperature fluctuations can be discerned, as well as advective episodes related to rainfall events that cause rapid temperature homogenization within the profile.

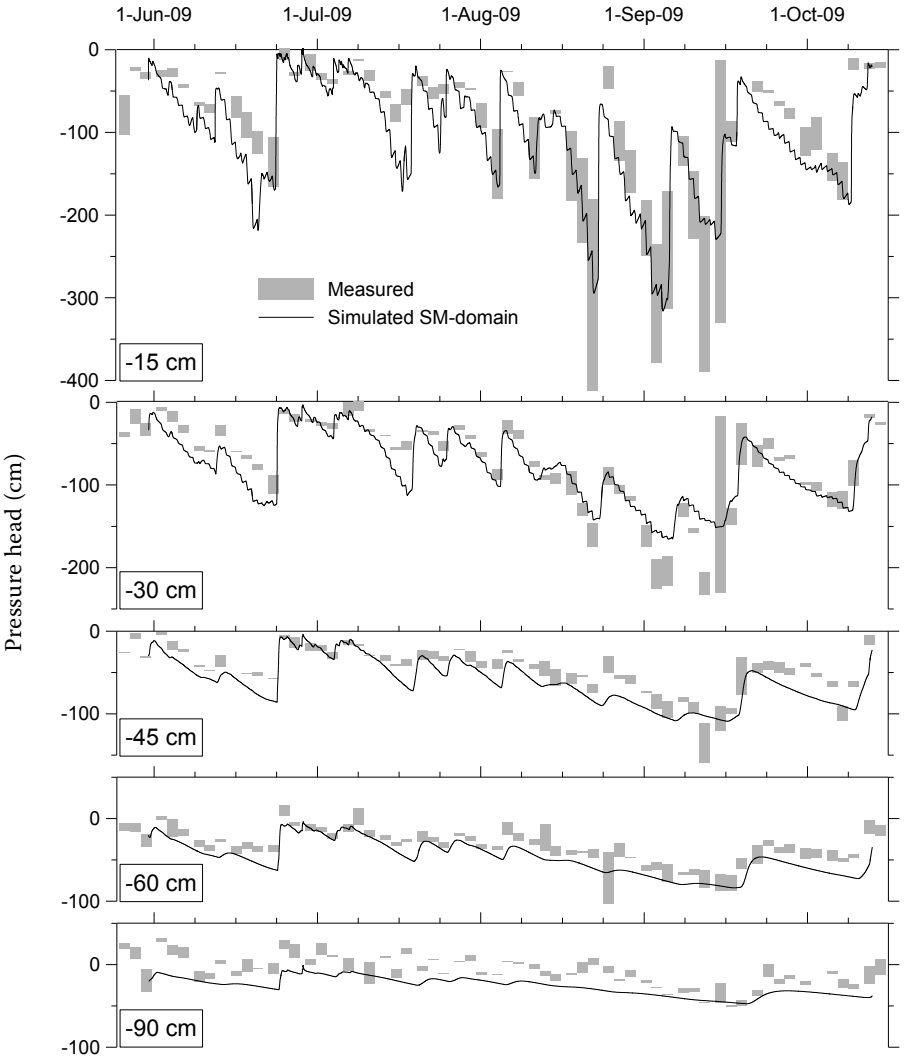

Figure 4. Soil water pressure heads measured (grey boxes showing ranges between the minimum and the maximum values observed) and simulated in SM-domain (solid line) at five different depths

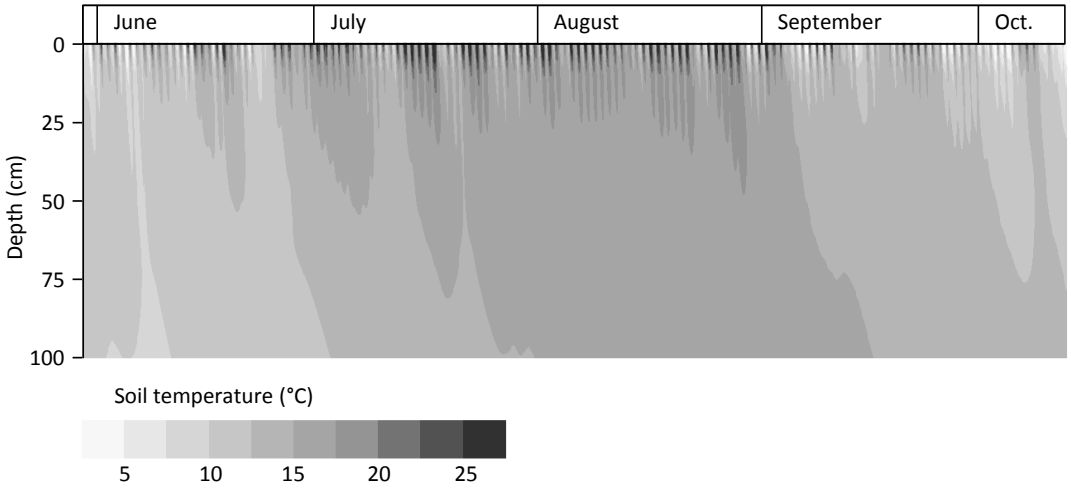

Figure 5. Spatiotemporal distribution of soil temperature simulated within the upper 100-cm soil profile

Simulated soil temperature distribution is compared with that observed in Figure 6. As in Figure 5, the results obtained with C&K λ(θ) approximation are presented. The quality of the soil temperature simulation as achieved with various λ(θ) estimation methods is evaluated in Table 3; mean error (ME), root-mean-square error (RMSE), and correlation coefficient (*R*) are presented.

For all λ(θ) estimation methods tested, while the overall temperature level was described relatively well at the depth 100 cm, it was underestimated throughout the upper 100-cm soil profile (see ME values in Table 3). From this point of view, differences between all three simulations are minute with the best results being achieved using C&H λ(θ) estimates. However, when more weight is given to larger errors, as in RMSE, the differences between the three simulations become more pronounced while C&K and LWS λ(θ) estimates stand out as more successful. The C&H-based simulation differs from the other two mainly in the predicted temperature oscillation amplitude; it greatly overestimates the short-term temperature variations near the soil surface and consequently also within the upper 50 cm of the soil profile. The temperature variations predicted by LWS and C&K-based simulations are far more realistic, although at a 5-cm depth the overestimation is also obvious. Correlation coefficient values (*R* in Table 3) illustrate that the simulated temperature variations are similar to those observed for both C&K and LWS λ(θ) estimates (Figure 6).

In the present study, the soil temperatures predicted using either LWS or C&K λ(θ) approximations are almost the same. It means that in our case the effect of considering or neglecting the nonlinearity of the relationship of soil thermal conductivity to soil water content is small. On the other hand,

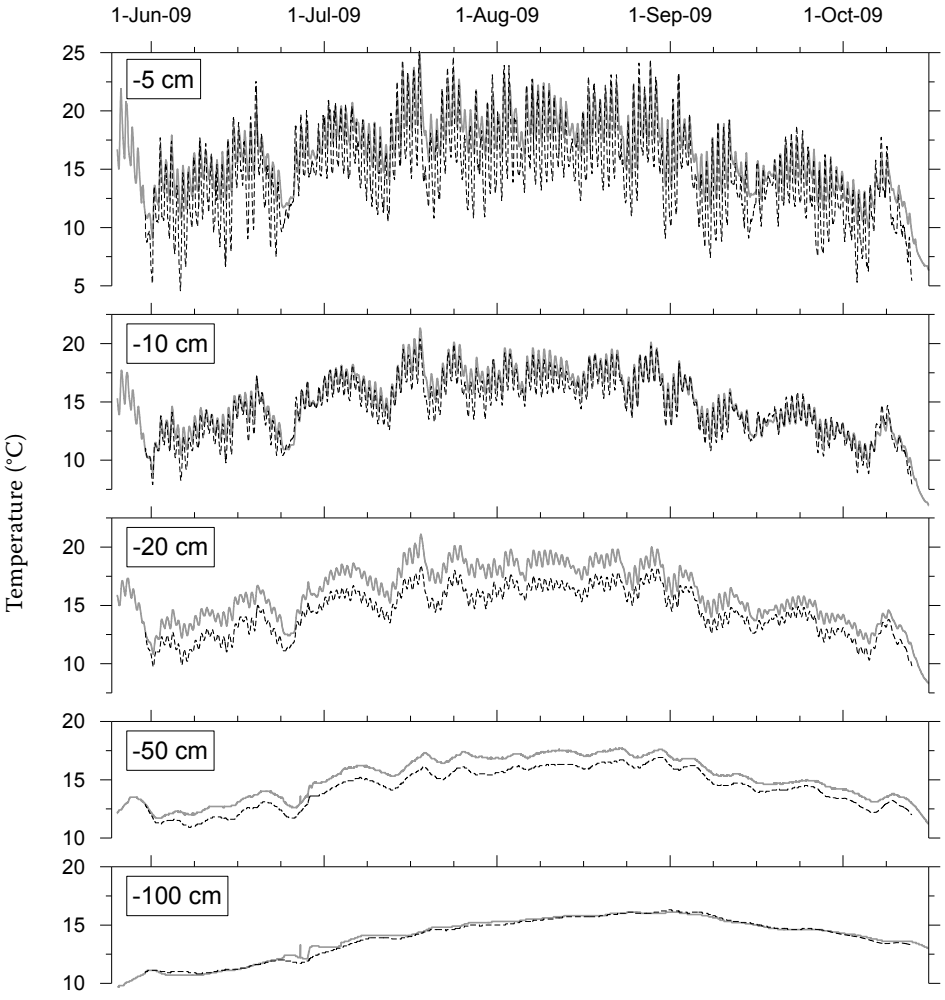

Figure 6. Soil temperatures measured (grey) and simulated in SM-domain (black dashed) at five different depths

Table 3. Comparison of soil temperature simulations achieved using different methods of the soil thermal conductivity estimation (C&K, LWS, and C&H): Mean Error (ME), Root Mean Square Error (RMSE) and correlation coefficient (*R*) are presented for five depths the temperature was measured at; the best results are highlighted

	Method	Depth (cm)				
		5	10	20	50	100
ME (°C)	C&K	–1.9	–0.5	–1.7	–0.9	–0.1
	LWS	–1.9	–0.5	–1.7	–0.9	–0.1
	C&H	**–1.8**	**–0.4**	**–1.6**	**–0.8**	**0.0**
RMSE (°C)	C&K	**2.5**	**0.8**	1.8	1.0	0.2
	LWS	2.6	0.9	**1.7**	0.9	**0.2**
	C&H	3.4	2.2	1.9	**0.9**	0.3
R (–)	C&K	**0.90**	**0.97**	0.98	0.99	0.99
	LWS	0.89	0.96	**0.98**	**0.99**	**0.99**
	C&H	0.81	0.82	0.92	0.97	0.98

the soil temperature simulation obtained by C&H λ(θ) estimation differs significantly. The difference observed within the upper 50 cm of the soil profile is mainly due to the difference in λ(θ) estimates for the uppermost soil layer (Figure 2) as C&H method does not provide the λ(θ) estimate for soils with high organic matter content. This difference is decreasing with depth, becoming negligible at the depth of 100 cm. However, contrasting λ(θ) estimates for the bottom soil layer (depths of 100 to 300 cm) resulted in a noticeable increase of differences in simulated temperatures with depth. Thus, while at the depth of 100 cm the seasonal temperature maximum predicted using C&H λ(θ) estimates is 0.1°C higher than that calculated using C&K λ(θ) approximation, it is 0.5°C lower at the depth of 300 cm.

Apart from the spatiotemporal temperature distribution, the model provides a detailed description of the soil heat fluxes. Thus, the soil surface conductive heat flux, Q_G, can be evaluated. In Figure 7a, all components of the soil surface energy balance (Eq. (11)) are presented for a two-day period (including a cloudy and a sunny day). Of those, the net radiation, R_N, was obtained by direct measurement; the latent heat flux, Q_L, was evaluated using Eq. (17); and Q_G was simulated using C&K λ(θ) estimates. It should be noted that

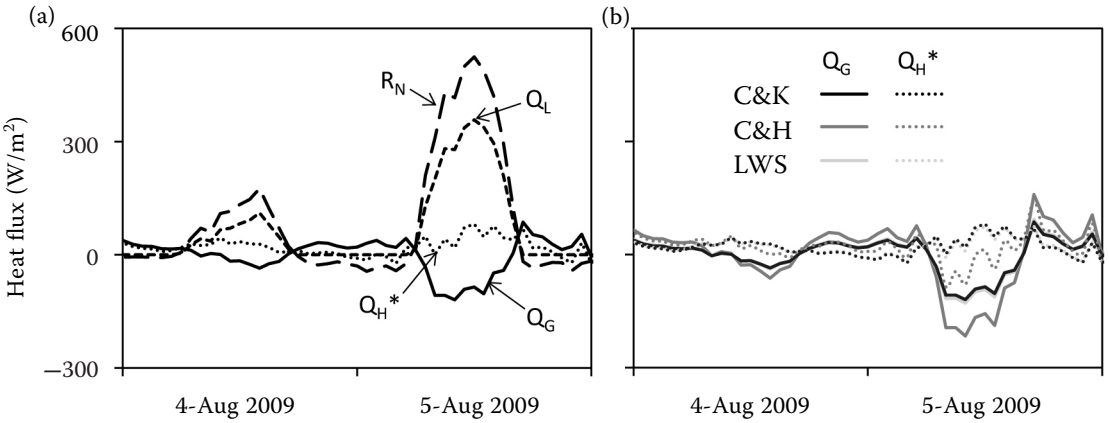

Figure 7. Surface energy fluxes on two typical days, cloudy and sunny: (a) all surface energy balance components as evaluated by C&K λ(θ): net radiation observed R_N, latent heat flux Q_L estimated using Eq. (17) , simulated conductive heat flux into soil Q_G, and the sensible heat flux calculated from the surface energy balance Q_H^*; (b) Q_G simulated and related Q_H^* as obtained using different λ(θ) approximations

an estimate of Q_G according to Allen *et al.* (1998) was used to calculate Q_L presented as well as the evapotranspiration rate applied as input in the simulation. The last component of the surface energy balance, the sensible heat flux, Q_H, can be approximately assessed based on micrometeorological data. Unfortunately, it was impossible to obtain a reliable estimate with the data available. Therefore, Q_H^* value presented in Figure 7 was calculated from the surface energy balance closure (i.e. $Q_H^* = R_N - Q_L - Q_G$). Consequently, errors of both Q_L and Q_G estimates are combined in Q_H^*. In the present study, these errors proved too big to allow Q_H^* to be considered a reasonable Q_H estimate.

In Figure 7b, Q_G estimates (solid lines) and respective Q_H^* values (dotted lines) as obtained using the three λ(θ) estimation methods are presented. The results obtained by C&K and LWS λ(θ) approximations are effectively the same. The Q_G fluxes calculated based on the C&H λ(θ) are substantially bigger. This difference is related to the higher soil thermal conductivity of the surface layer when estimated by the C&H relationships (Figure 2). The overestimation of the actual surface soil heat flux is rather serious, as the related Q_H^* becomes negative during the sunny day (implying a downward sensible heat flux), which is obviously wrong. It can be concluded that in terms of the surface soil heat flux prediction the C&H methodology failed due to its inability to describe the thermal conductivity of the surface layer. The fact that dense vegetation roots in topsoil may significantly reduce thermal conductivity, consequently affecting the surface energy fluxes, was previously recognized e.g. by Yang *et al.* 2005.

While the differences in the simulation results obtained using different λ(θ) approximations do not seem significant in terms of the soil temperature, they are substantial when the surface soil heat flux is regarded. These differences are considerable not only at the time-scale of diurnal variation, as seen in Figure 7, but also at the seasonal time-scale. Taken cumulatively, over the period when the soil was warming up (May 30–August 29), the cumulative Q_G calculated by C&H λ(θ) was by 19.3% greater than that obtained by C&K λ(θ).

Figure 8 summarizes the heat fluxes within the upper 100-cm soil profile. It shows how the heat entering the profile through the soil surface due to both conduction Q_G and advection was partly discharged to the subsoil (44% by PF-domain, 9% by SM-domain) and partly taken away via the root water uptake (47%). The major portion of the downward transfer was passed through the PF-domain following the intensive rainfall events at the end of June. The heat loss associated with both the SM-domain drainage and the root water uptake was evenly distributed in time. The soil heat storage at the end of the period simulated was approximately the same as at the beginning.

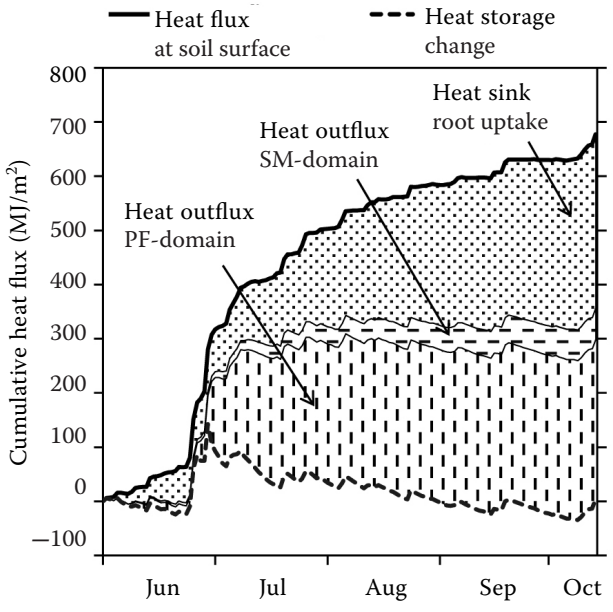

Figure 8. Heat balance of the upper 100-cm soil profile; the heat influx includes both conducted heat Q_G and advected heat entering the soil with rainwater

SUMMARY AND CONCLUSIONS

Soil thermal conditions during the vegetation season 2009 were simulated using a dual-continuum model of coupled water and heat transport. For this purpose, the soil thermal conductivity as a function of the soil water content, λ(θ), had to be assessed. No experimental evaluation of this parameter was available for the soil studied. Three λ(θ) estimation methods of varying complexity were selected (Chung & Horton 1987; Côté & Konrad 2005; Loukili *et al.* 2008). Each method was applied without making any additional adjustments to improve the model performance. The unknown values of thermal conductivities of the soil constituents (used in the last two methods) were taken from literature (Côté & Konrad 2005).

In the case presented, a more realistic soil temperature simulation was achieved using the two

λ(θ) estimation methods that use the information on the soil composition to predict the saturated soil thermal conductivity (LWS and C&K methods). The main advantage was that these methods provide lower thermal conductivity values for soils with high organic matter content, as is the case of the top layer of grass-covered soil profile. Thermal conductivities of the soil constituents, needed as input, can be sufficiently well estimated based on values found in literature. These would also provide ranges to stay in, should λ(θ) be optimized. In that case, the adaptability of λ(θ) shape in C&K estimation method can also be helpful.

The soil heat flux simulation results are greatly influenced by the depth of the soil profile included in the model and by the bottom boundary condition applied. In the present study, a 3-meter-deep soil profile with zero conductive heat flux at its bottom was used.

The model dual character essentially affects the heat flux simulation. The extent of this influence depends on the actual soil profile hydraulic and thermal properties as well as on the boundary conditions. In the present case, the PF-domain effect on the soil temperature was mostly negligible except for a few days following the major rainfall events at the end of June. Mechanisms by which the PF-domain influences the simulated soil temperature are threefold. First, the soil heat conduction is affected as the soil thermal conductivities in both domains essentially differ. The impact diminishes as the PF-domain fraction decreases. Second, the water flow through the PF-domain affects the heat advective flux. During a rainfall event, the excessive water of temperature given by the surface conditions passes relatively rapidly through the PF-domain while tending to equilibrate with the surrounding SM-domain. Consequently, the reaction to the soil surface temperature propagates into deeper parts faster. Third, the hydraulic functioning of PF-domain influences the soil water distribution and thus the soil thermal conductivity profile. Consequently, both advective and conductive soil heat fluxes are affected. In the present study, the latter mechanism had the highest effect.

It should be noted that the simulated soil thermal conditions are strongly affected by the root water uptake approximation. Due to the intensive diurnal fluctuations of the soil temperature near the soil surface, the timing and vertical distribution of the root water uptake within this region not only affects the temperature of the water withdrawn but also controls the soil thermal conductivity near the soil surface. This topic is a possible subject for further research.

Acknowledgements. The research was funded by the Czech Science Foundation, Grant No. 205/08/1174.

References

Allen R.G., Pereira L.S., Raes D., Smith M. (1998): Crop Evapotranspiration. Guidelines for Computing Crop Water Requirements. FAO Irrigation and Drainage Paper 56, FAO, Rome.

Bauer J., Weihermüller L., Huisman J.A., Herbst M., Graf A., Séquaris J.M., Vereecken H. (2012): Inverse determination of heterotrophic soil respiration response to temperature and water content under field conditions. Biogeochemistry, **108**: 119–134.

Buchner J.S., Šimůnek J., Lee J., Rolston D.E., Hopmans J.W., King A.P., Six J. (2008): Evaluation of CO_2 fluxes from an agricultural field using a process-based numerical model. Journal of Hydrology, **361**: 31–143.

Chung S.-O., Horton R. (1987): Soil heat and water flow with a partial surface mulch. Water Resources Research, **23**: 2175–2186.

Císlerová M. (2005): Preferential flow in the vadose zone of Cambisols. In: Šír M. *et al.* (ed.): Hydrology in a Small Watershed 2005. Institute of Hydrodynamics ASCR, Prague, 23–30. (in Czech)

Côté J., Konrad J.M. (2005): A generalized thermal conductivity model for soils and construction materials. Canadian Geotechnical Journal, **42**: 443–458.

de Marsily G. (1986): Quantitative Hydrogeology. Academic Press, London.

de Vries D.A. (1963): Thermal properties of soils. In: van Wijk W.R. (ed.): Physics of Plant Environment. North-Holland Publ., Amsterdam.

Dohnal M., Dusek J., Vogel T. (2010): Improving hydraulic conductivity estimates from minidisk infiltrometer measurements for soils with wide pore-size distributions. Soil Science Society of America Journal, **74**: 804–811.

Feddes R.A., Kowalik P.J., Zaradny H. (1978): Simulation of Field Water Use and Crop Yield. Centre for Agricultural Publishing and Documentation, Wageningen.

Gerke H.H., van Genuchten M.Th. (1993): A dual-porosity model for simulating the preferential movement of water and solutes in structured porous media. Water Resources Research, **29**: 305–319.

Hillel D. (1998): Environmental Soil Physics. Academic Press, San Diego.

Ju W.M., Chen J.M., Black T.A., Barr A.G., Liu J., Chen B.Z. (2006): Modelling multi-year coupled carbon and water fluxes in a boreal aspen forest. Agricultural and Forest Meteorology, **140**: 136–151.

Loukili Y., Woodbury A.D., Snelgrove K.R. (2008): SABAE-HW: An enhanced water balance prediction in the Canadian Land Surface Scheme compared with existing models. Vadose Zone Journal, **7**: 865–877.

Monteith J.L. (1981): Evaporation and surface temperature. Quarterly Journal of the Royal Meteorological Society, **107**: 1–27.

Ronan A.D., Prudic D.E., Thodal C.E., Constantz J. (1998): Field study and simulation of diurnal temperature effects on infiltration and variably saturated flow beneath an ephemeral stream. Water Resources Research, **34**: 2137–2153.

Sakai M., Jones S.B., Tuller M. (2011): Numerical evaluation of subsurface soil water evaporation derived from sensible heat balance. Water Resources Research, **47**: W02547.

Tesař M., Balek J., Šír M. (2006): Hydrological research in the Volyňka basin (Bohemian forest, Czech Republic). Journal of Hydrology and Hydromechanics, **54**: 137–150. (in Czech)

Timlin D.J., Pachepsky Y., Acock B.A., Šimůnek J., Flerchinger G., Whisler F.D. (2002): Error analysis of soil temperature simulations using measured and estimated hourly weather data with 2DSOIL. Agricultural Systems, **72**: 215–239.

Vogel T., van Genuchten M.Th., Cislerova M. (2001): Effect of the shape of soil hydraulic properties near saturation on numerical simulation of variably-saturated flow. Advances in Water Resources, **24**: 133–144.

Vogel T., Brezina J., Dohnal M., Dusek, J. (2010): Physical and numerical coupling in dual-continuum modeling of preferential flow. Vadose Zone Journal, **9**: 260–267.

Vogel T., Dohnal M., Votrubova J. (2011): Modeling heat fluxes in macroporous soil under sparse young forest of temperate humid climate. Journal of Hydrology, **402**: 367–376.

Yang K., Koike T., Ye B.S., Bastidas L. (2005): Inverse analysis of the role of soil vertical heterogeneity in controlling surface soil state and energy partition. Journal of Geophysical Research-Atmospheres, **110**: D08101.

Received for publication May 23, 2012
Accepted after corrections June 27, 2012

Corresponding author:

Ing. Jana Votrubová, Ph.D., České vysoké učení technické v Praze, Fakulta stavební, Thákurova 7, 166 29 Praha 6, Česká republika
e-mail: jana.votrubova@fsv.cvut.cz